Journal of the Iranian Chemical Society (2024) 21:211–225
https://doi.org/10.1007/s13738-023-02919-2

ORIGINAL PAPER

Durable magnetite-chitosan core–shell nanoparticles as reusable green nanocatalyst for the benign one-pot three-component synthesis of spirooxindoles and spirochromenes at ambient temperature under both solvent-free and ultrasonic conditions in aqueous ethanol solution

Pegah Mardaneh[1] · **Ali Reza Sardarian**[1]

Received: 27 July 2023 / Accepted: 28 October 2023 / Published online: 26 November 2023

Abstract
In the present research, a novel, efficient, and green nanocatalyst has been afforded by coating Fe_3O_4 nanoparticles with chitosan through simple and readily available chemicals. Fourier-transform infrared spectroscopy, X-ray diffraction, scanning electron microscopy, dynamic light scattering, vibrating sample magnetometer, and thermogravimetric analyses were used to describe this nanocatalyst. The catalytic performance of the Fe_3O_4@chitosan heterogeneous nanocatalyst was investigated in an environmentally benign and efficacious fabrication of a variety of spirooxindole and spirochromene derivatives in high yields via employing three-component reactions of malononitrile, dimedone, and isatin in a solvent-free medium (Method A) and under ultrasonic conditions in EtOH/H_2O (Method B) at ambient temperature. The achieved nanocatalyst could be easily removed from the mixture of the reaction and was recyclable seven times via a simple external magnet without appreciable loss in catalytic proficiency. Several other advantages of this methodology were environmental friendliness, simple operation, excellent yields, economical handling, and easy workup.

✉ Ali Reza Sardarian
sardarian@shirazu.ac.ir

[1] Chemistry Department, College of Sciences, Shiraz University, Shiraz 71946 84795, Iran

Graphical abstract

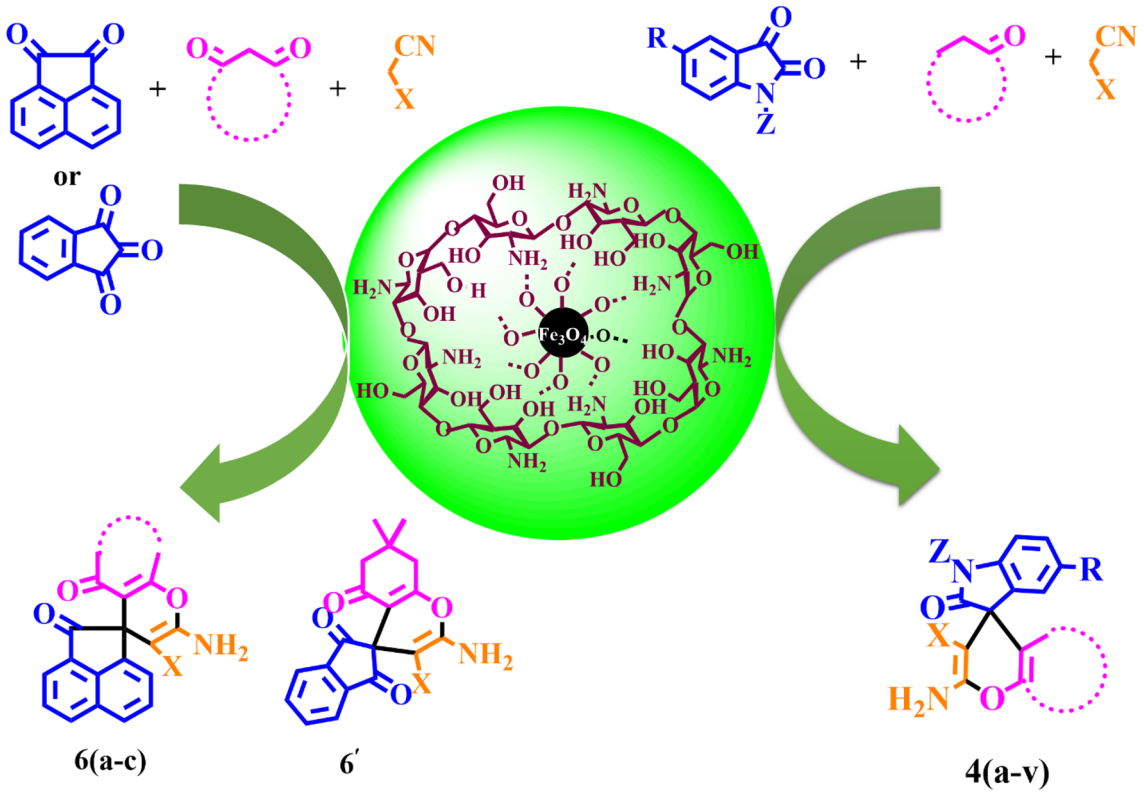

Keywords Superparamagnetic · Green nanocatalyst · Spirooxindoles · Spirochromenes · Solvent-free · Ultrasonic condition

Introduction

Nanocatalysis has brought a revolution in the field of catalysis and plays a crucial role in green organic synthesis. This emerging catalytic technique possesses several merits over conventional catalysts, such as a high surface-to-volume ratio, great catalytic performance, high selectivity, and stability. A fundamental approach to achieve catalysts with exceptional features is the production of heterogeneous nanocatalysts. Although the catalytic activity of homogeneous nanocatalysts is high, their complete separation from the reaction medium is not easy and can be troublesome, especially in the pharmaceutical industry. However, heterogeneous nanocatalysts can be rapidly and readily isolated from the reaction mixture and reused without any loss in amount during the purification process [1–4].

Owing to the nanoscale size of the nanocatalysts, their isolation from the reaction mixture and reuse them are challenging tasks, which can lead to waste of a large amount of catalyst. To overcome this issue, employing magnetic nanoparticles (MNPs) or nanosupports is the best solution due to easy isolation by magnetic separation. Fe_3O_4 nanoparticles (NPs) are at the highest point of attention for their use as nanocatalysts due to magnetic fractures (superparamagnetism), non-toxicity, great surface area, biocompatibility, oxidative stability, and easy synthesis and handling. These NPs have been widely employed in catalysis, biomedicine, magnetic resonance imaging (MRI), separation technology, and the environment sector. The co-precipitation process using Fe (II) and Fe (III) ions is the most common procedure to synthesize Fe_3O_4 magnetic (NPs) [5–7]. Despite all of the significant features of Fe_3O_4 (NPs), their dispersion in the reaction mixture is limited, and they accumulate to large clusters, which leads to a decrease in catalytic efficiency. Hence, covering these NPs with various materials, including natural polymers such as polysaccharides, prevents their aggregation. Natural polymers are the best choice to cover NPs and lead to green nanoscale composites as new green nanocatalysts for promoting a wide range of organic reactions [7]. On the other side, green chemistry, as an emerging field of sustainable sciences, as well as technologies, assists in the usage of renewable feedstocks as sustainable resources. Therefore, developing novel heterogeneous nanocatalysts based on biodegradable and green supports

has attracted considerable attention due to increasing concern about environmental pollution. Chitosan, as a safe and biologically renewable material with attractive properties including biocompatibility, biodegradability, antibacterial properties, non-toxicity, non-antigenicity, bioactivity, readly availability, and inexpensiveness, has been used in various domains such as medicine, pharmaceutical pharmaceutics, as well as industry. This biopolymer is appropriate for designing new functionalized nanocomposites [8–10].

More than 90% of the active ingredients used in the pharmaceutical industry, phytochemistry, and veterinary medicine are heterocyclic compounds. Spiro heterocycles with distinct biological activities play a superior role in modern organic and medicinal chemistry, among which spirocyclic oxindoles are promising candidates for drug discovery. This type of compound exists in natural products and biologically active molecules and constitutes both oxindoles and other heterocyclic moieties simultaneously. Anti-inflammatory, anti-oxidant, anti-cancer, anti-microbial, and anti-tubercular activity are demonstrated by spirooxindole systems. On the other hand, spirochromenes are produced when C-3 in spirooxindoles is shared with the pyran ring, which is an oxygen-containing heterocyclic fused with the spirooxindole ring system. These compounds display valuable properties including anti-cancer, anti-anaphylactic, anti-coagulant, diuretic, and spasmolytic performances [11–17]. The biological potential of these spiro-based compounds motivates researchers to invent efficient chemical processes. Figure 1 displays the chemical compositions of a few physiologically active spirooxindoles, including Spirotryprostatin A (cell cycle regulator), Pteropodine (rat muscarinic receptor), and Ciapargamin (antimalarial drug) [18].

Recently, heterocyclic systems have been produced through a three-component condensation reaction using malononitrile, isatin, and enolizable CH-acids in the presence of various catalysts. Multi-component reactions (MCRs) are dominant as platforms for the sustainable synthesis of heterocyclic compounds due to their green chemistry features, environmental friendliness, operational simplicity, inherent atom economy, and high selectivity [19–23]. Various catalytic systems have been employed for the synthesis of spiro heterocycles like urea, potassium phthalimide, amino acids, biopolymers, organic bases, inorganic salts, metal oxides, and ionic liquids [24–27]. Aluminum sulfate–sulfuric acid [28], dabco-based ionic liquids [29], Fe_2O_3/VO_2 [30], SiO_2@g-C_3N_4 nanocomposite [31], copper ferrite nanoparticles [32], nano-cellulose [33], collagen-Fe_3O_4 [34], cellulose/Ag nanocomposite [35], nano MgO [36], tris-hydroxymethylamino methane (THAM) [11], TiO_2 nanoparticles [37], $Bi_2Fe_4O_9$ (NPs) [38], (Fe_3O_4/COS@β-CD-SO_3H nanoparticles) [39], $CoFe_2O_4$@SiO_2 [40], $InCl_3$ [41], poly(ethylene glycol) [42, 43], triethylbenzylammonium chloride (TEBA) [44], ammonium salt [45], TBAB [46], L-proline [47, 48], oxalic acid dihydrate: proline LTTM [49], Silica-bonded N-propyl sulfamic acid [50] are the examples of these catalytic systems.

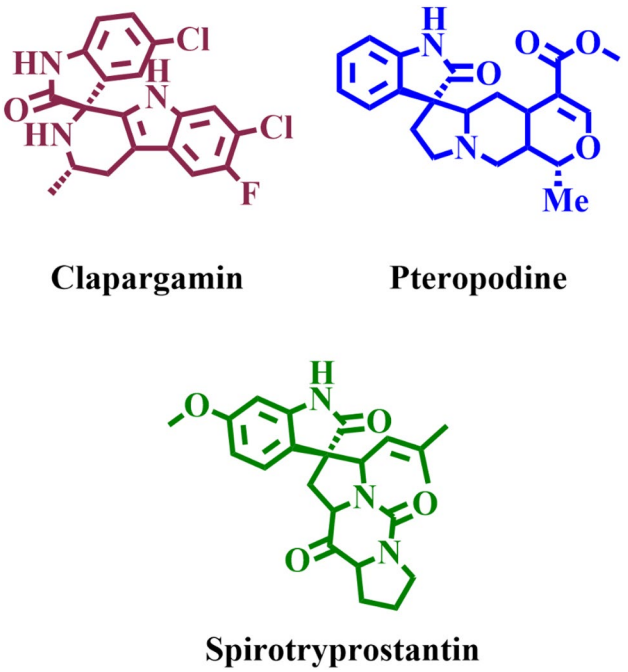

Fig. 1 Examples of spirooxindole compounds with biologically active properties

Current research findings revealed the uses of chitosan and Fe_3O_4 nanoparticles as nanomagnetic catalysts for the preparation of various heterocyclics. Fe_3O_4@chitosan-tannic acid nanocomposite was employed as a heterogeneous nanocatalyst for the fabrication of pyranopyrazoles [7]. Some of the advantages of this study were economically affordable, eco-friendliness, mild reaction conditions, and high yields. In another study, nano-Fe $_3O_4$@chitosan as a superior and retrievable heterogeneous catalyst was designed for benzopyranophenazines preparation [51]. Maleki and co-workers noted a synthetic protocol for the synthesis of benzimidazoles/benzodiazepines in the presence of reusable Fe_3O_4/chitosan nanocatalyst [52]. Also, Fe_3O_4/chitosan as a green nanocatalyst was applied to synthesize 2,3-dihydroquinazolin-4(*1H*)-ones [53]. Furthermore, benzimidazolo[2,3-b] quinazolinone derivatives with excellent yields were produced by Fe_3O_4@chitosan as an eco-friendly and reusable nanocatalyst [9].

Sonochemistry has attracted significant interest in chemistry study fields during the last few decades. Sonochemical synthesis, as a major and environmentally friendly strategy, has numerous advantageous effects in synthetic organic chemistry, which has led organic chemists to focus on its usage for synthesizing organic chemicals [54]. Therefore, instead of utilizing heat as a source of energy, ultrasonic

irradiation is an alternative. Ultrasound-aided reactions progress through the phenomena of acoustic cavitation, which involves emergence, expansion, and dissolution of bubbles in the liquid medium [55].

Our main concern is to develop a sustainable nanocatalyzed synthetic methodology for preparing spirooxindoles and spirochromenes compounds. Considering the principles of green chemistry, we have decided to utilize Fe_3O_4@chitosan as a green, biocompatible, heterogeneous nanomagnetic catalyst, which can be easily recovered magnetically, under solvent-free and ultrasonic conditions for synthesizing these classes of compounds.

Results and discussion

Magnetic Fe_3O_4 nanoparticles (NPs) were generated by coprecipitation procedure modification. Coating of Fe_3O_4 (NPs) with chitosan was carried out by modifying the described procedures in the literature [56, 57]. Chitosan dissolves in an acidic solution through protonation and conversion to polycations, which is dependent on the pH of the solution. Chitosan is precipitated onto the surface of Fe_3O_4 to create Fe_3O_4@chitosan nanoparticles as support when the solution's pH is changed to pH = 14 by adding an aqueous solution of NaOH (Scheme 1). This occurs due to the strong hydrogen bonding between protonated chitosan and negatively charged Fe_3O_4 nanoparticles.

Then nano-Fe_3O_4@chitosan were characterized by Fourier transform infrared (FT-IR), thermogravimetric analysis (TGA), X-ray diffraction (XRD), scanning electron microscopy(SEM), dynamic light scattering, and (DLS) and vibrating sample magnetometer (VSM). The XRD patterns of pure Fe_3O_4 and Fe_3O_4@chitosan nanocatalysts are presented in Fig. 2. As can be observed, the Fe_3O_4 (NPs) exhibit a highly crystalline cubic spinel structure, which agrees very well with the conventional XRD spectrum for Fe_3O_4 (cubic phase) [57]. The characteristic peaks for pure Fe_3O_4 NPs were observed at $2\theta = 30.4°$, 35.5°, 43.4°, 53.8°, 57.3°, and 62.9°. These peaks were labeled by their respective indices (220), (311), (400), (422), (511), and (440). The identical characteristic peaks of Fe_3O_4 are seen in the XRD spectrum after being coated with chitosan, which is evidence for maintaining the crystalline structure and successful coating of Fe_3O_4 nanoparticles.

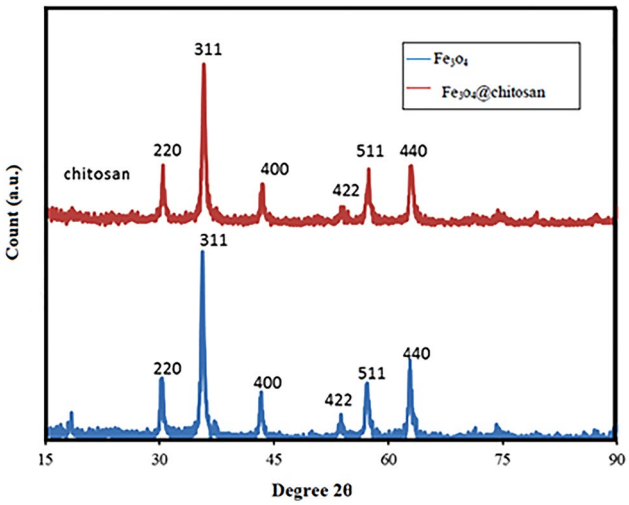

Fig. 2 XRD pattern of pure Fe_3O_4@chitosan nanoparticles and pure Fe_3O_4

The FT-IR spectra of Fe_3O_4@chitosan, Fe_3O_4 (NPs), and chitosan appear in Fig. 3. The FT-IR spectrum of Fe_3O_4 (NPs) exhibits the characteristic peaks at 580 cm^{-1} (Fe–O) and 3423 cm^{-1} (O–H stretching) (Fig. 3a). The FT-IR spectrum of chitosan (Fig. 3b) contains characteristics: (a) N–H stretching and bending bands at 3440 and 1635, cm^{-1}, (b) O–H and C–O stretching bands of primary alcoholic groups at 2854 and 1319 cm^{-1}, and (c) C–H stretching band at 2923 cm^{-1}. The presence of all of the characteristic bands of Fe_3O_4 nanoparticles and chitosan (with slight shifts) in the FT-IR spectrum Fe_3O_4 wrapped with chitosan is another indication for Fe_3O_4@chitosan production (Fig. 3c).

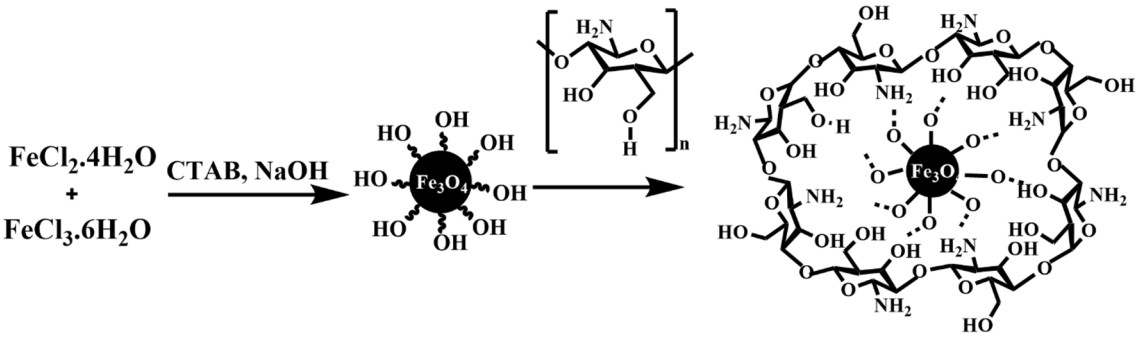

Scheme 1 Fe_3O_4@chitosan preparation schematic diagram

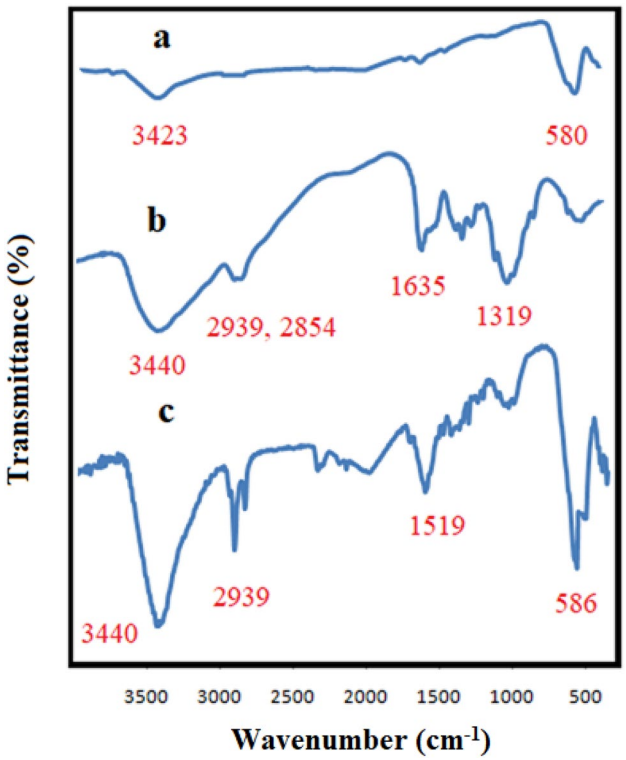

Fig. 3 FT-IR spectra of Fe_3O_4 **a**, chitosan **b**, and Fe_3O_4@chitosan **c**

Thermogravimetric analysis was performed to determination of the loading amount of the nanocatalyst and evaluate the material's thermal stability. As seen in Fig. 4, the thermogravimetric (TG) data have been reported in the form of TG% and TG mg, differential thermogravimetric (DTG), and differential thermogravimetric analysis (DTA). This study exhibits three weight loss stages. The first stage, which occurs at 25 °C–200 °C, is related to the loss of humidity and solvent stuck in the nanocatalyst. In the second stage at 200 °C [58], the decomposition of chitosan is observed which is equal to 0.30 mg weight loss (10%). The third decomposition stage appeared at 380 °C–480 °C because of the decomposition of Fe_3O_4 which is equal to 0.2 mg weight loss (3.3%) and other moieties were related to ionization polymers. These results also confirm the successful coating of the surface of Fe_3O_4 with chitosan.

Fe_3O_4 and Fe_3O_4@chitosan morphology and particle size were monitored by SEM, as shown in Fig. 5. These images demonstrate that Fe_3O_4 NPs with 10–12 nm particle size (Fig. 5a) and Fe_3O_4@chitosan particles with the size of 30–35 nm have retained the morphological properties and size of Fe_3O_4 nanoparticles, which is an indication of uniformly wrapping of Fe_3O_4 NPs with chitosan (Fig. 5b). The average size of the nanoparticle was characterized by dynamic light scattering (DLS) and confirmed the ~ 30 nm as the approximate average size (Fig. 6).

Fe_3O_4@chitosan particles were tested by VSM, and the result shows a magnetic field of up to 8000 Oe at a

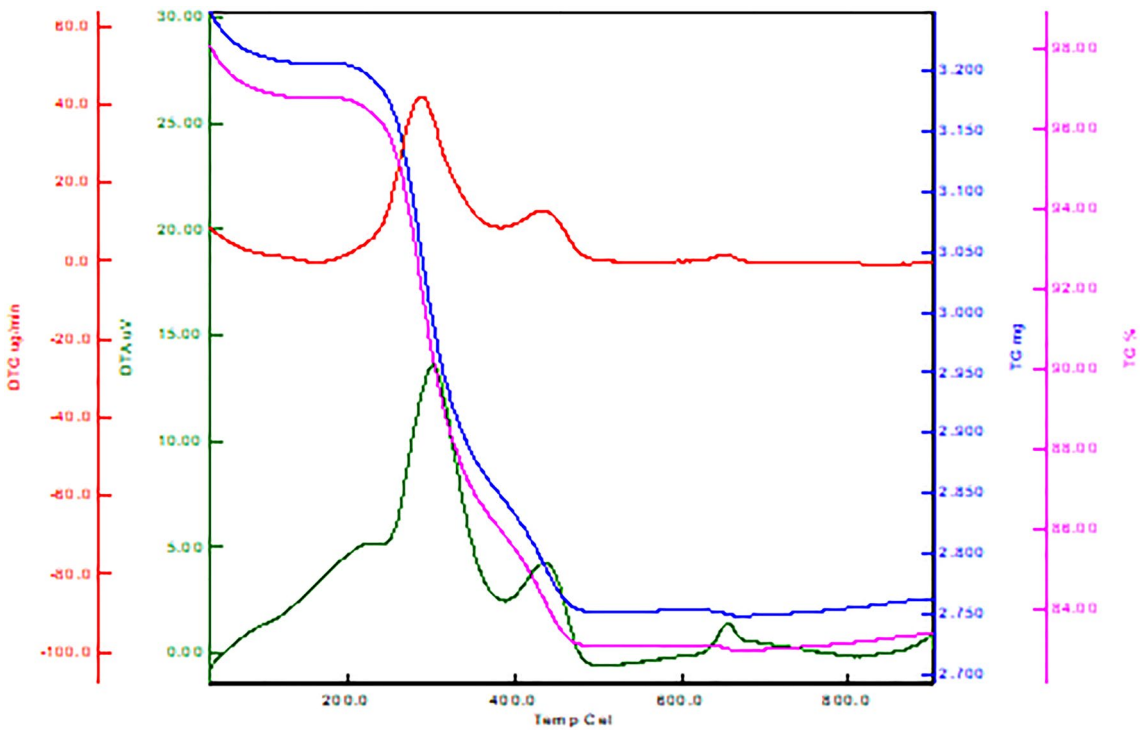

Fig. 4 TG (blue), TG % (pink), DTG (red), and DTA (green) data of Fe_3O_4@chitosan

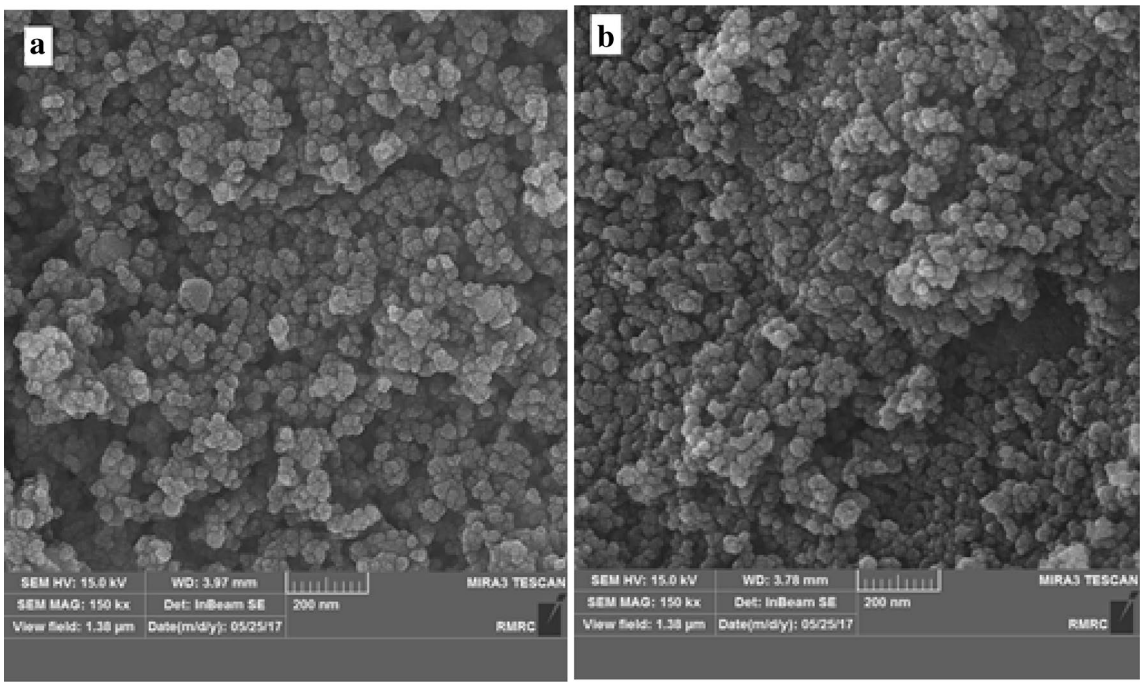

Fig. 5 SEM images of pure Fe_3O_4 **a** and Fe_3O_4@chitosan nanoparticle **b**

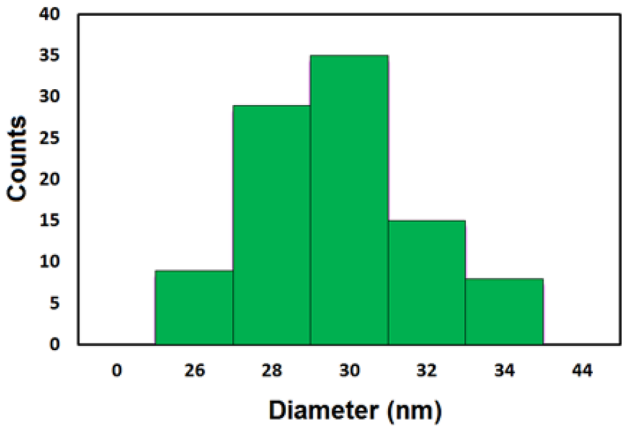

Fig. 6 DLS image of Fe_3O_4@chitosan (NPs)

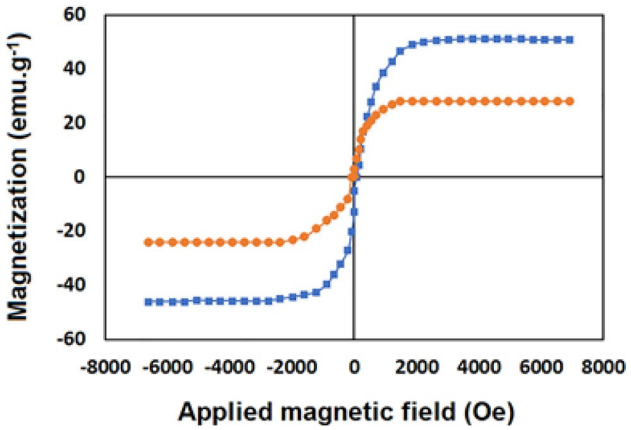

Fig. 7 VSM image of Fe_3O_4 **a** and Fe_3O_4@chitosan **b**

temperature of 300 K (Fig. 7). According to magnetic experiments, the saturation magnetization of nano-Fe_3O_4 and nano-Fe_3O_4@chitosan are 51.5 and 28.2 emu g^{-1}, respectively (Fig. 7). These findings indicate that magnetism behavior remained even after coating and functionalization.

In addition, the elemental analysis of the Fe_3O_4@chitosan demonstrated C: 6.23%, N: 1.06%, and H: 0.82% is equal to 10% loading chitosan, which is in good agreement with the results provided by TGA analysis.

Having prepared and characterized the Fe_3O_4@chitosan nanocatalyst, we initially optimized the reaction parameters. In the presence of a catalytic concentration of Fe_3O_4@chitosan (30 mg), the reaction between isatin, dimedone, and malononitrile was selected as a model reaction (Scheme 2).

The effects of temperature, catalyst concentration, and solvent were investigated to determine the most efficient conditions and the optimal reaction parameters. The corresponding data are presented in Table 1.

To verify the role of Fe_3O_4@chitosan NPs in the preparation of the corresponding spirooxindole, the model reaction was evaluated in the presence of chitosan, Fe_3O_4, and also in the absence of the nanocatalyst. The spirooxindole 4a was obtained in 68% after half an hour and 28% in four hours in the presence of chitosan and Fe_3O_4, respectively (Table 2,

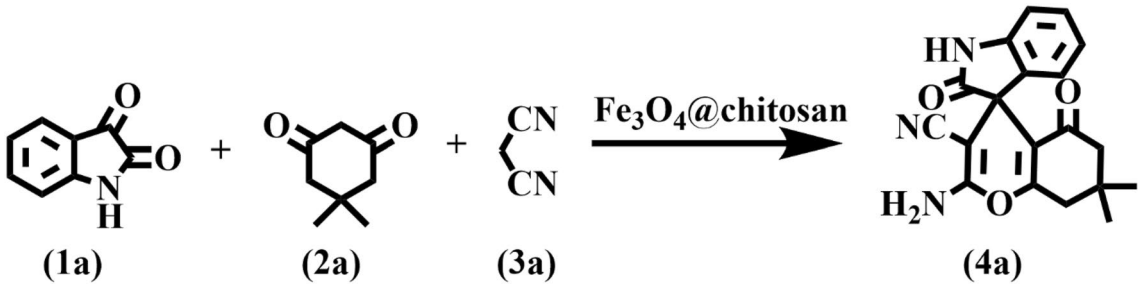

Scheme 2 Model reaction for the synthesis of spirooxindole derivatives

Table 1 The reaction parameters optimization for the synthesis of spirooxindole 4a [a]

Entry	Catalyst (mg)	Solvent	Temp (°C)	Time (min)	Yield (%)
1	Fe_3O_4@Chitosan (50)	EtOH	R.T	< 5	51
2	Fe_3O_4@Chitosan (50)	EtOH/H_2O (1:1)	R.T	< 5	62
3	Fe_3O_4@Chitosan (50)	H_2O	R.T	< 5	75
4	Fe_3O_4@Chitosan (50)	CH_2Cl_2	R.T	240	40
5	Fe_3O_4@Chitosan (50)	$CHCl_3$	R.T	240	47
6	Fe_3O_4@Chitosan (50)	Acetonitrile	R.T	240	34
7	Fe_3O_4@Chitosan (50)	Ethyl acetate	R.T	240	42
8	Fe_3O_4@Chitosan (10)	Solvent free	R.T	< 5	78
9	Fe_3O_4@Chitosan (20)	Solvent free	R.T	< 5	84
10	Fe_3O_4@Chitosan (30)	Solvent free	R.T	< 5	87
11	Fe_3O_4@Chitosan (40)	Solvent free	R.T	< 5	92
12	**Fe_3O_4@Chitosan (50)**	**Solvent free**	R.T	**< 2**	**97**
13	Fe_3O_4@Chitosan (55)	Solvent free	R.T	< 5	97
14	Chitosan (50)	Solvent free	R.T	30	68
15	Fe_3O_4 (50)	Solvent free	R.T	240	28
16	–	Solvent free	R.T	240	–

[a]Reaction conditions: Isatin (1.0 mmol), dimedone (1.0 mmol), malononitrile (1.0 mmol), Fe_3O_4@chitosan, room temperature, solvent (5 mL)

entries 14 and 15) but the desired product was not formed in the lack of catalyst (Table 2, entry 16). The efficiency of different amounts of catalyst was tested and it was clarified that the best result is provided when 0.05 g of Fe_3O_4@chitosan is loaded (Table 2, entry 12), and employing a higher amount does not produce any enhancement in the activity of the catalyst (Table 2, entry 13) and lower amounts have resulted in lower yields (Table 2, entries 8–11). Therefore, the optimized reaction condition is the usage of 0.05 g of Fe_3O_4@chitosan at room temperature under solvent-free media.

To explore the effect of ultrasonic technique on the catalytic activity of Fe_3O_4@chitosan in the preparation of 2-amino-7,7-dimethyl-2′,5-dioxo-5,6,7,8-tetrahydrospiro[chromene-4,3′-indoline]-3-carbonitrile, the reaction among isatin, malononitrile and dimedone was selected as the model reaction, then solvent and catalyst effects were studied.

First, the reaction was examined in water in the absence of the nanocatalyst. Monitoring the reaction with TLC showed all of the starting material remained intact after 8 h at room temperature under ultrasonic conditions (Table 2, entry 1). Then, the reaction was performed in H_2O, EtOH, and different mixtures of EtOH and H_2O at room temperature under ultrasonic conditions in the presence of 250 mg Fe_3O_4@chitosan (Table 2, Entries 2–6). When the model reaction was performed in EtOH after 3.5 h, Fe_3O_4@chitosan demonstrated the highest efficiency (Table 2, entry 3). The similar results were also obtained in H_2O: EtOH (1:1) and H_2O: EtOH (4:1) although the reaction took place in longer reaction time (5 h) in these mixtures (Table 2, entries 4 and 5). Regarding the economic and environmental issues, the mixture of H_2O: EtOH (4:1) was chosen as the best solvent. Then, the effect of the nanocatalyst amount was studied. When the lower amount of the nanocatalyst was used, the reaction was completed in a longer reaction time (Table 2, entry 7). Increasing the nanocatalyst concentration has no significant effects on the reaction conditions (Table 2, entry 6).

Table 2 Optimization of three-component coupling reaction among isatin, dimedone, and malononitrile for synthesis of spirooxindole **4a** under ultrasonic condition[a]

Entry	Catalyst (mg)	Solvent	Temp (°C)	Time (h)	Yield [b]of 4a (%)
1	–	H_2O	R.T	8	–
2	Fe_3O_4@Chitosan (250)	H_2O	R.T	8	84
3	Fe_3O_4@Chitosan (250)	EtOH	R.T	3.5	90
4	**Fe_3O_4@Chitosan (250)**	**H_2O/EtOH (4:1)**	**R.T**	**5**	**90**
5	Fe_3O_4@Chitosan (250)	H_2O/EtOH (1:1)	R.T	5	90
6	Fe_3O_4@Chitosan (275)	H_2O/EtOH (4:1)	R.T	5	90
7	Fe_3O_4@Chitosan (200)	H_2O/EtOH (4:1)	R.T	9.5	90
8	Chitosan (250)	H_2O/EtOH (4:1)	R.T	8	65
9	Fe_3O_4 (250)	H_2O/EtOH (4:1)	R.T	12	25

[a]Reaction condition: isatin (5.0 mmol), dimedone (5.0 mmol), malononitrile (5.0 mmol), solvent (100 mL) and Fe_3O_4@chitosan as nanocatalyst (250 mg) under ultrasonic condition

[b]The yield of isolated product

To determine the scope and versatility of Fe_3O_4@chitosan NPs at room temperature under solvent-free and ultrasonic conditions for the production of spirooxindoles, a variety of isatins and C–H acidic compounds such as dimedone, 1,3-cyclohexadione, barbituric acid, *N,N*-dimethyl barbituric acid, thiobarbituric acid, 6-chloro-4- hydroxycoumarin, 4-hydroxycoumarin, and 2-hydroxynaphthalene-1,4-dione (2a-2 h) were treated with malononitrile or ethyl 2-cyanoacetate in the presence of Fe_3O_4@chitosan (Table 3).

Having obtained excellent results, we extended the generality of this protocol for the one-pot three-component synthesis of spirochromenes with the replacement of isatin with acenaphthylene-1,2-dione (5) and ninhydrin (5′) under similar reaction conditions. All of the experiments were conducted with excellent yields (Table 4).

Scheme 3 illustrates the suggested mechanism for the synthesis of spirooxindole derivatives (such as 4a) utilizing Fe_3O_4@chitosan as a nanocatalyst. Initially, the amino groups on the surface of Fe_3O_4@chitosan are protonated by the malononitrile to provide the corresponding carbanion (7). Then, the produced carbanion attacks to the carbonyl group of isatin, which is protonated by the ammonium salt of chitosan. This step was treated as a fast Knoevenagel condensation. Next, the compound (8) is produced through several steps including dehydration, Michael reaction on α, β-unsaturated nitrile by the corresponding enol in the reaction mixture, and intramolecular nucleophilic addition on the nitrile groups. Finally, the desired product (4a) is produced by the tautomerization of the compound (9) (Table 3).

When solid catalysts are used in chemical reactions, the reusability and recovery of the nanocatalyst become crucial factors. Isatin, dimedone, and malononitrile were used in a model reaction with the magnetic nanocatalyst Fe_3O_4@chitosan NPs for the recycling investigation. The reactivity of the nanocatalyst was not significantly altered after seven cycles of recycling, and the yield decreased only slightly with each additional cycle (Fig. 8).

Following the seven-time runs, the recovered Fe_3O_4@chitosan nanocatalyst was once again characterized through FT-IR, XRD, DLS, and SEM (Figs. 9, 10, 11 and 12). According to Fig. 9, the characteristic peaks at 586 cm^{-1} (Fe–O), 3440 cm^{-1} (O–H and N–H stretching) 1519 cm^{-1} (C–O stretching), and 2939 cm^{-1} (C–H stretching) are represented in appropriate condition. Figure 10 demonstrates that the crystalline structure of Fe_3O_4 nanoparticles is maintained after seven-time recycling. Due to the number of NP aggregations throughout the recycling process, the size of NPs was exhibited at 26–38 nm by DLS analysis (Fig. 11). Finally, the SEM image showed that the size of NPs was not changed after several recycling (Fig. 12). These investigations showed that the Fe_3O_4@chitosan NPs are a durable and effective catalyst for multicomponent reactions.

To demonstrate the nanocatalyst's advanced capability, the current catalytic system was compared to a few different systems used for the synthesis of spirooxindoles in MCR reactions. As shown in Table 5, it is clear that the presented approach has positive advantages including environmental friendliness, simple operation, excellent yields, economical handling, and easy workup.

Table 3 Synthesis of spirooxindole derivatives

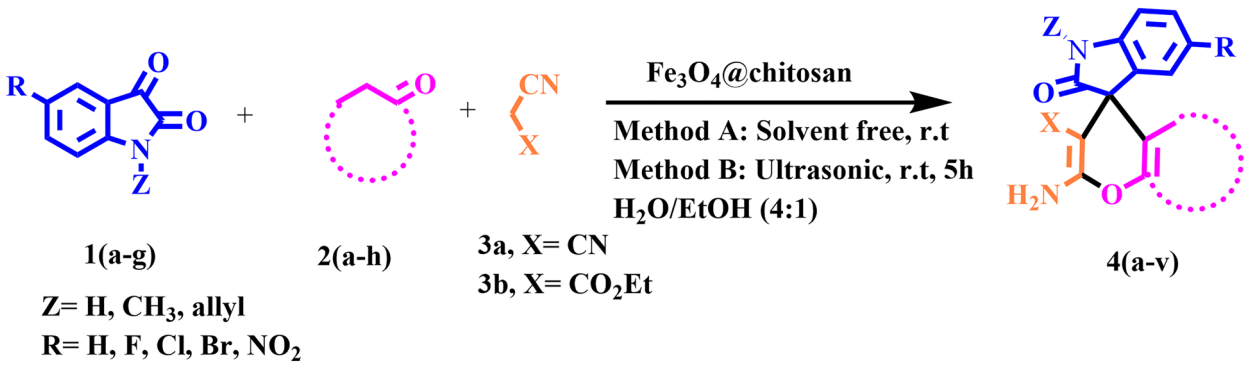

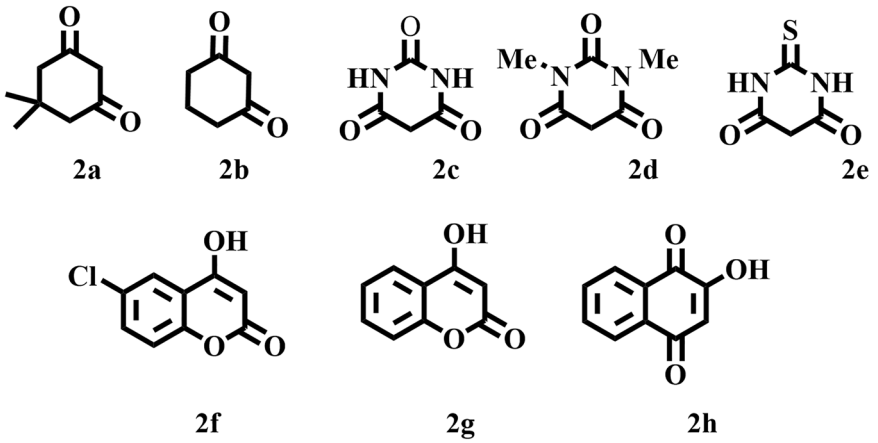

Entry	R	Z	C–H acidic	X	Product	Time (min)		Yield (%)		M.P. (°C)	
						Method A	Method B	Method A	Method B	Found	Reported
1	H	H	2a	CN	4a	< 2	300	96	88	269–271	268–270 [45]
2	H	Allyl	2a	CN	4b	3	300	97	82	256–258	–
3	NO_2	H	2a	CN	4c	< 1	300	97	84	306–308	302–304 [43]
4	Br	H	2a	CN	4d	2.5	300	85	80	305–307	> 300 [48]
5	Cl	H	2a	CN	4e	3.5	300	88	83	302–304	> 300 [48]
6	F	H	2a	CN	4f	3.5	300	94	89	272–274	276–277 [50]
7	Br	Allyl	2a	CN	4 g	6[a]	300	93	87	240–243	–
8	H	H	2a	CO_2Et	4 h	45	300	92	78	259–261	256–258 [48]
9	H	CH_3	2a	CN	4i	< 2	300	94	89	252–254	255–258 [49]
10	H	H	2b	CN	4j	11	300	96	85	300–302	298–299 [48]
11	H	Allyl	2b	CO_2Et	4 k	49	300	94	89	217–220	-
12	H	H	2c	CN	4 l	18	300	84	78	278–280	273–275 [46]
13	NO_2	H	2c	CN	4 m	35	300	91	86	304–306	> 300 [49]
14	F	H	2c	CN	4n	27	300	88	82	263–265	–
15	H	H	2d	CN	4o	20	300	91	86	228–230	226–229 [49]
16	Cl	H	2d	CN	4p	15	300	92	85	253–255	251–253 [49]
17	Br	H	2d	CN	4q	15	300	95	80	303–305	> 300 [49]
18	H	H	2e	CN	4r	30	300	90	85	244–246	238–242 [44]
19	H	Allyl	2e	CN	4 s	15	300	94	89	250–253	–
20	H	H	2f	CN	4t	35	300	89	92	217–220	–
21	H	H	2 g	CN	4u	45	300	85	86	252–254	250 [41]
22	H	H	2 h	CN	4v	50	300	89	90	262(dec)	250(dec) [46]

[a]Method A) Isatin derivative (1.0 mmol), C-H acidic compounds (1.0 mmol), malononitrile or ethyl 2-cyanoacetate (1.0 mmol), solvent free, Fe_3O_4@chitosan (50 mg) at R.T

Table 3 (continued)

[b]Method B) Isatin derivative (5.0 mmol), C-H acidic (5.0 mmol), malononitrile or ethyl 2-cyanoacetate (5.0 mmol), H_2O/EtOH (4:1) (100 mL) and Fe_3O_4@chitosan (250 mg) in ultrasonic condition at R.T

[c]Isolated yields

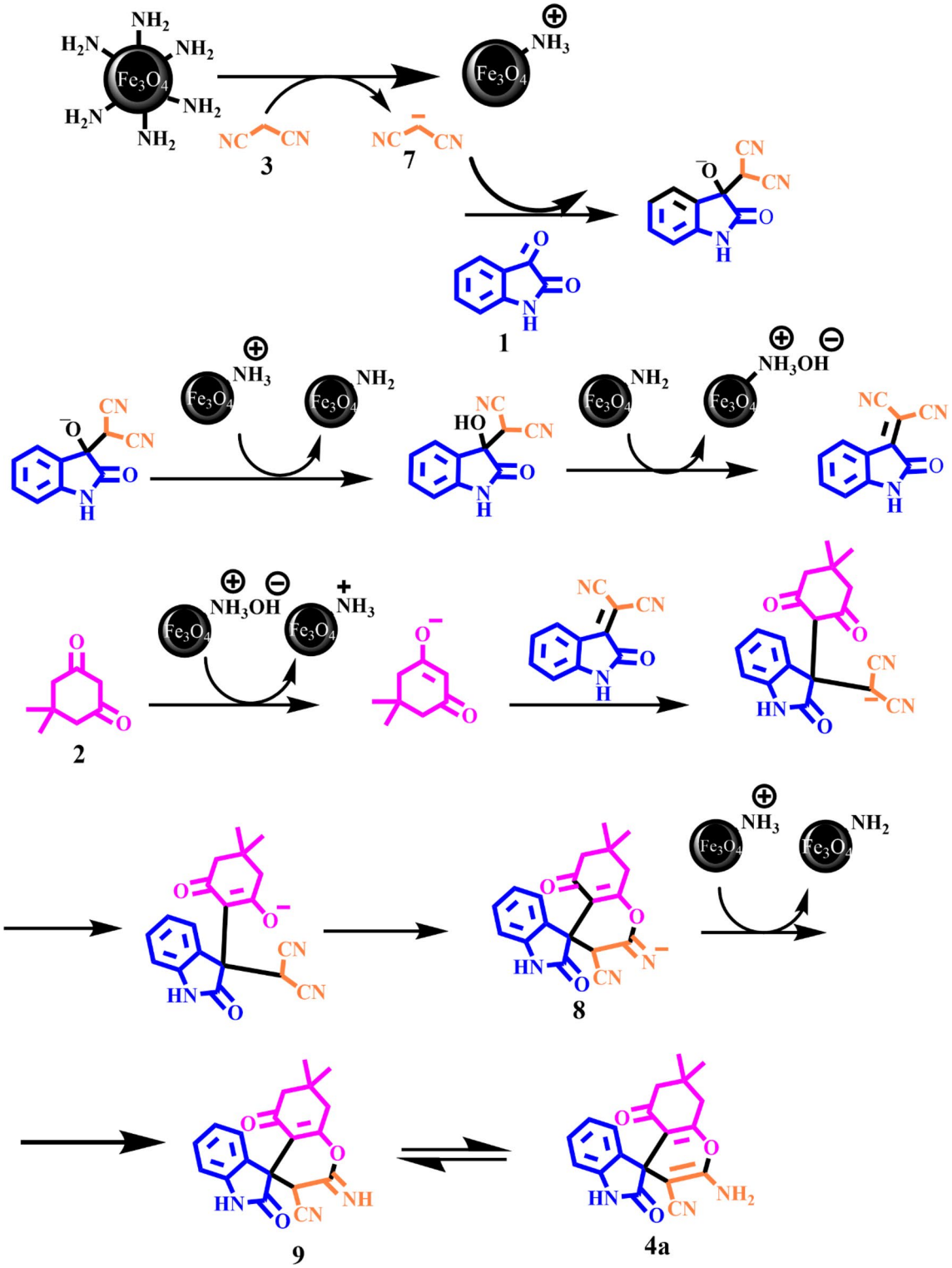

Scheme 3 Fe_3O_4@chitosan as a heterogeneous catalyst for the synthesis of 4a: a probable mechanism nanocatalyst

Table 4 Synthesis of spirochromene derivatives.[a]

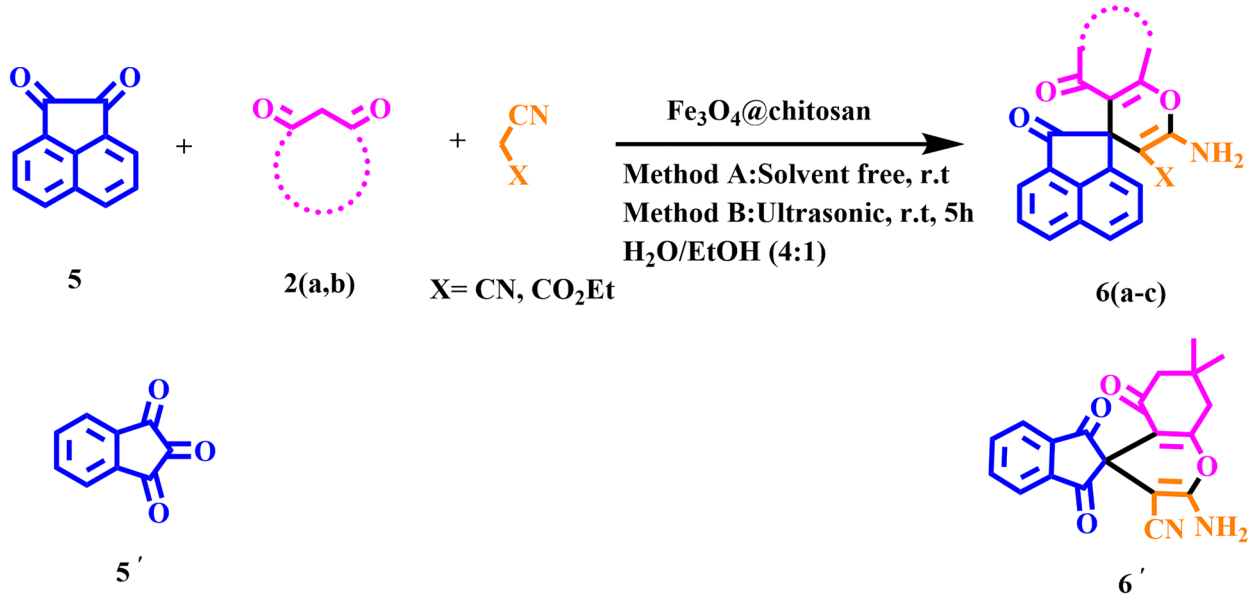

Entry	1,3-Diketone	X	Product	Time (min)		Yield (%)		M.P. (°C)	
				Method A	Method B	Method A	Method B	Found	reported
1	2a	CN	6a	15	300	94	90	263–265	260–262 [44]
2	2b	CN	6b	23	300	88	84	246–248	245–247 [44]
3	2b	CO_2Et	6c	42	300	89	89	229–231	225–227 [44]
4	2a	CN	6′	8	300	93	87	292–294	290–292 [59]

[a]Reaction conditions: Acenaphtoquinone (1.0 mmol) and ninhydrin (1.0 mmol), 1,3-dicarbonyl (1.0 mmol), malononitrile or ethyl 2-cyanoacetate (1.0 mmol), Fe_3O_4@chitosan (50 mg), solvent-free, at R.T

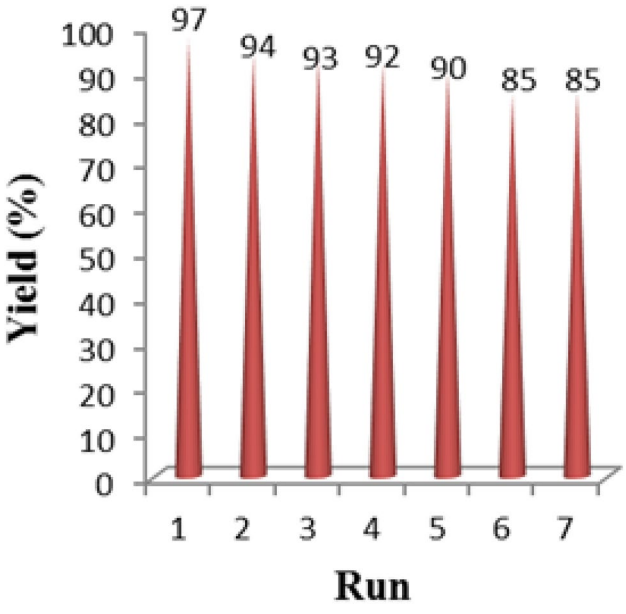

Fig. 8 Recyclability of Fe_3O_4@chitosan in the synthesis of spirooxindole derivatives

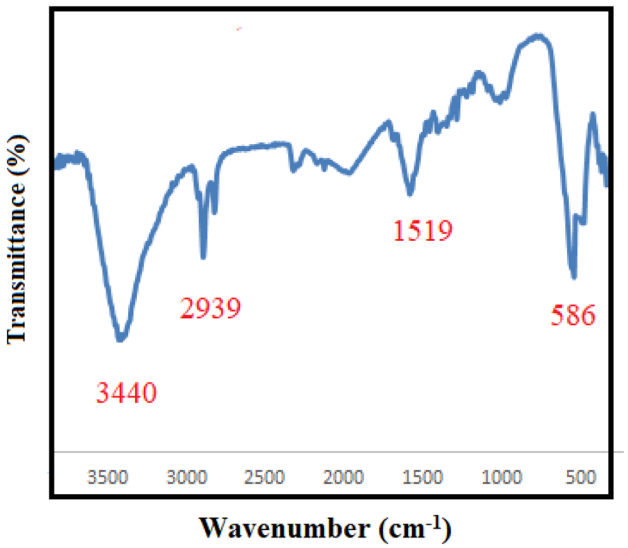

Fig. 9 FT-IR spectrum after seven-time recycling

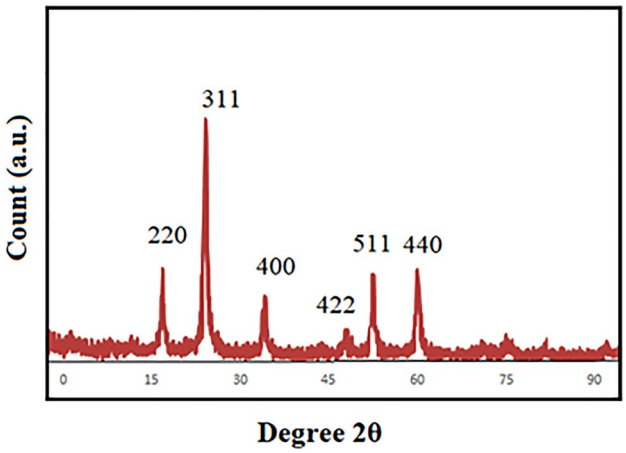

Fig. 10 XRD spectrum after seven-time recycling

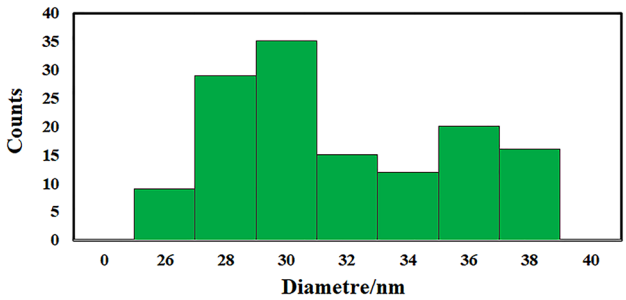

Fig. 11 DLS chart after seven-time recycling

Conclusion

In a brief explanation, a novel and green heterogeneous magnetic nanocatalyst was synthesized by coating magnetic Fe_3O_4 NPs with chitosan, as a green and natural component, through an easy procedure and readily available and low-cost materials. The most significant aspect of this nanocatalyst was biodegradability due to its biodegradable polymer. The prepared nanocatalyst was characterized by XRD, SEM, TGA, FT-IR, VSM, and DLS analyses. By employing the catalytic amount of this nanocatalyst, a variety of spirooxindole and spirochromene derivatives were developed via three-component reactions of isatin derivatives/acenaphtoqunone, cyclic C-H acid compound, and malononitrile/ethyl 2-cyanoacetate under solvent-free condition at room temperature and in H_2O/EtOH (4:1) under ultrasonic condition. Owing to the magnetic performance of the Fe_3O_4/chitosan nanocatalyst originated from the nano-Fe_3O_4, the achieved nanocatalyst could be simply separated from the reaction mixture, and it was recyclable seven times via a simple external magnet without appreciable loss in catalytic proficiency. Following the principle

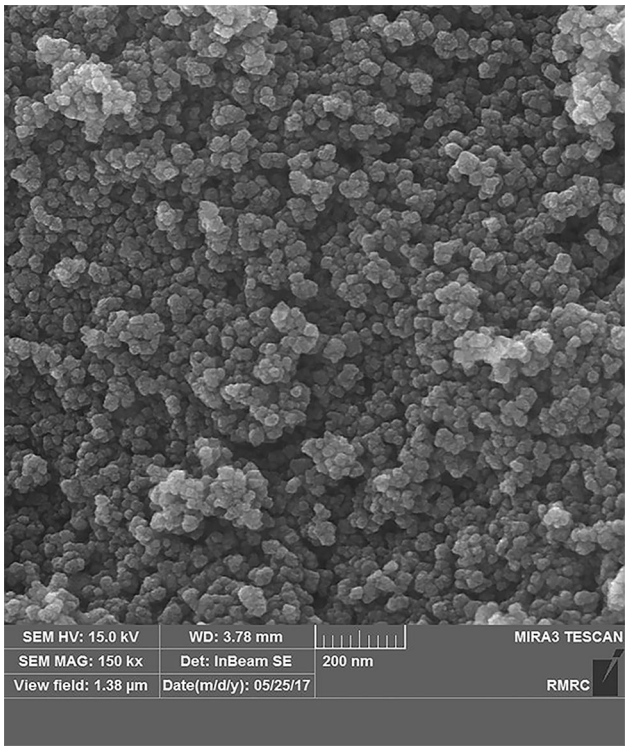

Fig. 12 SEM image after seven-time recycling

of green chemistry, Fe_3O_4/chitosan has considered factors like an easy workup procedure, excellent yields, reusable catalysts, and environmentally friendly reaction conditions that performed the synthesis of this important class of biologically active compound in a short reaction time.

Experimental section

General information

Merck, Aldrich, and Fluka were the suppliers of the chemicals used in this study. All the solvents were distilled, dried, and purified by standard process. NMR spectra were recorded on a Bruker Avance DPX 250 and 400 MHz spectrometer in DMSO-d_6 using tetramethylsilane (TMS) as an internal reference. The synthetic compounds were investigated by Fourier-transform infrared spectroscopy (FT-IR) analysis using a Shimadzu FT-IR 8300 spectrophotometer, and tablets were formed by compressing the sample with KBr. Magnetic nanoparticles' crystalline polymer and structural stability were investigated using a Bruker AXS D8-advanced X-ray diffractometer with Cu Ka radiation ($\lambda = 1.5418$). Thermal analysis of the samples was conducted using TG/DTA instrument in a Perkin-Elmer Pyris Diamond model thermal analyzer. In a nitrogen gas flow with a heating rate of 10 °C min^{-1}, the measurements were recorded

Table 5 Fe_3O_4@chitosan is compared to various catalysts described in the literature for the synthesis of spirooxindole derivatives

Entry	Catalyst	Condition	Time (min)	Yield(%	References
1	[Dabco-H]Cl	ACN/ 50 °C	60	88	29
2	$Al_4(SO_4)_6{\cdot}(H_2SO_4){\cdot}24H_2O$	H_2O/ 80 °C	20	99	28
3	Nano-cellulose-$SBCL_5$	EtOH/ Reflux	15	96	33
4	Fe_3O_4/COS@β-CD-SO_3H	H_2O/ 50 °C	20	98	39
5	$CoFe_2O_4$@SiO_2	EtOH: H_2O/ 80 °C	5	98	40
6	PC/AgNPs	H_2O/EtOH/ Reflux	10	94	35
7	$Bi_2Fe_4O_9$	H_2O/ 80 °C	10	97	38
8	Fe_3O_4@SiO_2 /ECH/IG	EtOH: H_2O / 60 °C	10	94	34
9	Fe_3O_4@chitosan	Solvent free/ r.t	< 2	98	This study

from room temperature to one thousand degrees Celsius. In platinum pans, samples ranging in weight from 1.5 to 3.5 mg were examined. The scanning electron microscope (SEM) was characterized using an FEI Quanta 200 SEM with a 20 kV acceleration voltage. Sonication was performed in hielscher, ultrasonic GmbH bath (Model-hielscher, operating frequency 30 kHz ± 10% and output power of 100 Watts). The magnetization of nanoparticles was estimated using a BHV-55 VSM, and DLS process was used to determine the size distribution profile by a HORIBA-LB 550 particle size analyzer. The mass spectra were captured using a Shimatzu GC–MS QP 1000 EX device.

Using thin-layer chromatography (TLC) on silica-gel polygram SILG/UV 254 plates, the purity of the substrate was determined and the reaction was controlled.

General procedure for the synthesis of Fe_3O_4

$FeCl_3.6H_2O$ (1.3 g, 4.8 mmol) and $FeCl_2{\cdot}4H_2O$ (0.9 g, 4.5 mmol) were combined and added to the solution of α-cetyl trimethylammonium bromide (CTAB) in water (500 mL), as a surfactant. The mixture was heated for 30 min at 80 °C. Then, a solution of NaOH (10 weight percent) was added drop by drop to the reaction mixture with mechanical stirring to create a black solid product until the pH of the reaction medium changed to 12. After that, the reaction mixture was heated for 1 h between 60–70 °C, and the black iron-oxide solid was filtered and washed with 5 mL water (3 times) and then dried at 80 °C for 10 h [60, 61].

Typical procedure for the synthesis of Fe_3O_4@chitosan nanoparticles

A mixture of 2.0 g Fe_3O_4 nanocrystal and 0.25 g of chitosan was rapidly mixed for 30 min in 50 mL of acetic acid aqueous solution (1% v/v) to provide a solution of Fe_3O_4 in chitosan. Following that, the chitosan-coated Fe_3O_4 nanoparticles were produced by adding 50 mL of 1 M NaOH solution. Deionized water was used to wash the final nanoparticles until the wash's pH reached 7 [56, 57].

Typical procedure for the synthesis of 2-amino-7,7-dimethyl-2′,5- dioxo-5,6,7,8-tetra hydrospiro[chromene-4,3′-indoline]-3-carbonitr ile derivation using solvent-free condition at room temperature (Method A)

A mixture of malononitrile (1.0 mmol, 0.066 g), isatin (1.0 mmol, 0.147 g), dimedone (1.0 mmol, 0.141 g), and Fe_3O_4@chitosan (0.05 g) were added to a round-bottomed flask at room temperature under a solvent-free condition, utilizing the minimum amount of ethanol (0.5 ml) with vigorous stirring for less than 2 min. Once the reaction was complete, the process was monitored by the thin-layer chromatography (TLC) method with the solvent mixture of *n*-hexane: ethyl acetate (2:1) and diluted with ethanol (5.0 mL). The catalyst was separated by an external magnet, and the product was filtered and washed with ethanol (2 × 5 mL). Finally, the solid product was crystallized with ethanol and water (3:1) to afford the pure spirooxindole.

Typical procedure for synthesis of 2-amino-7,7-dim ethyl-2′,5-dioxo-5,6,7,8-etrahydrospiro[chromene-4 ,3′-indoline]-3-carbonitrile derivation using ultrasonic condition (Method B)

A mixture of isatin (5.0 mmol, 0.735 g), or acenaphtoquinone (5.0 mmol, 0.91 g), malononitril (5.0 mmol, 0.33 g), dimedone (5.0 mmol, 0.705 g) and Fe_3O_4@chitosan (0.25 g) in 100 mL H_2O/EtOH (4:1), was sonicated for 5 h at room temperature. The reaction progress was monitored by TLC (*n*-hexane:ethyl acetate; 2:1) until the starting substrates were completely consumed. The catalyst was removed by an external magnet from the reaction mixture and then washed with ethanol (2 × 5 mL). Finally, the solid product was crystallized from a mixture of ethanol and water (3:1) to afford the pure spirooxindole.

Supplementary Information The online version contains supplementary material available at https://doi.org/10.1007/s13738-023-02919-2.

Acknowledgements The authors acknowledge financial support from the research council of Shiraz University and are grateful for financial support from the Council of Iran National Science Foundation**.**

Declarations

Conflict of interest The authors declare that they have no known competing financial interests or personal relationships that could have appeared to influence the work reported in this paper.

References

1. N. Rahman, R. Nongkhlaw, Org. Chem. **6**, 272–313 (2018). https://doi.org/10.24820/ark
2. F. Kalantari, A. Ramazani, M.R. Poor Heravi, H. Aghahosseini, K. Ślepokura, Inorg. Chem. **60**, 15010–15023 (2021). https://doi.org/10.1021/acs.inorgchem.1c02470
3. A.K. Rathi, R. Zboril, R.S. Varma, M.B. Gawande, A.C.S. Symp, Series **1238**, 39–78 (2016). https://doi.org/10.1021/bk-2016-1238.ch002
4. M. Narasimhan, M. Chandrasekaran, S. Govindasamy, A. Aravamudhan, J. Environ. Chem. Eng. **9**, 104876 (2021). https://doi.org/10.1016/j.jece.2020.104876
5. S. Liu, B. Yu, S. Wang, Y. Shen, H. Cong, Adv. Colloid Interface Sci. **281**, 102165 (2020). https://doi.org/10.1016/j.cis.2020.102165
6. A. Maleki, F. Hassanzadeh-Afruzi, Z. Varzi, M.S. Esmaeili, Mater. Sci. Eng. C **109**, 110502 (2020). https://doi.org/10.1016/j.msec.2019.110502
7. M. Kamalzare, M.R. Ahghari, M. Bayat, A. Maleki, Sci. Rep. **11**, 1–10 (2021). https://doi.org/10.1038/s41598-021-99121-2
8. M. Dohendou, K. Pakzad, Z. Nezafat, M. Nasrollahzadeh, M.G. Dekamin, Int. J. Biol. Macromol. **192**, 771–819 (2021). https://doi.org/10.1016/j.ijbiomac.2021.09.162
9. A. Maleki, M. Aghaei, N. Ghamari, Chem. Lett. **44**, 259–261 (2015). https://doi.org/10.1246/cl.141074
10. Y.V.D. Nageswar, N.L.C. Domingues, R. Katla, Polysaccharides (2021). https://doi.org/10.1002/9781119711414.ch25
11. S.S. Khot, P.V. Anbhule, U.V. Desai, P.P. Wadgaonkar, Comptes Rendus Chim. **21**, 814–821 (2018). https://doi.org/10.1016/j.crci.2018.05.005
12. B. Yu, D.Q. Yu, H.M. Liu, Eur. J. Med. Chem. **97**, 673–698 (2015). https://doi.org/10.1016/j.ejmech.2014.06.056
13. K. Ramakumar, T. Maji, J.J. Partridge, J.A. Tunge, Org. Lett. **19**, 4014–4017 (2017). https://doi.org/10.1021/acs.orglett.7b01752
14. N. Ye, H. Chen, E.A. Wold, P.Y. Shi, J. Zhou, A.C.S. Infect, Dis. **2**, 382–392 (2016). https://doi.org/10.1021/acsinfecdis.6b00041
15. M.M. Heravi, T. Momeni, M. Mirzaei, V. Zadsirjan, M. Tahmasebi, Inorg. Nano-Metal. Chem. **51**, 896–909 (2021). https://doi.org/10.1080/24701556.2020.1813172
16. L.M. Zhou, R.Y. Qu, G.F. Yang, Expert Opin. Drug Discov. **15**, 603–625 (2020). https://doi.org/10.1080/17460441.2020.1733526
17. J.P. MacDonald, J.J. Badillo, G.E. Arevalo, A. Silva-García, A.K. Franz, A.C.S. Comb, Sci. **14**, 285–293 (2012). https://doi.org/10.1021/co300003c
18. M. Baghernejad, S. Khodabakhshi, S. Tajik, New J. Chem. **40**, 2704–2709 (2016). https://doi.org/10.1039/C5NJ03027G
19. P. Brandão, C.S. Marques, E.P. Carreiro, M. Pineiro, A.J. Burke, Chem. Rec. **21**, 924–1037 (2021). https://doi.org/10.1002/tcr.202000167
20. M.V. Murlykina, A.D. Morozova, I.M. Zviagin, Y.I. Sakhno, S.M. Desenko, V.A. Chebanov, Front. Chem. **6**, 1–43 (2018). https://doi.org/10.3389/fchem.2018.00527
21. A. Chaudhary, P. Saluja, G. Khanna, *Green Chemistry in Environmental Sustainability and Chemical Education* (Springer, Singapore, 2018), pp.15–21. https://doi.org/10.1007/978-981-10-8390-7_2
22. C.J. Gerry, S.L. Schreiber, Curr. Opin. Chem. Biol. **56**, 1–9 (2020). https://doi.org/10.1016/j.cbpa.2019.08.008
23. W.R.J.D. Galloway, A. Isidro-Llobet, D.R. Spring, Nat. Commun. **1**, 1–13 (2020). https://doi.org/10.1038/ncomms1081
24. S. Nagaraju, B. Paplal, K. Sathish, S. Giri, D. Kashinath, Tetrahedron Lett. **58**, 4200–4204 (2017). https://doi.org/10.1016/j.tetlet.2017.09.060
25. S.M. Baghbanian, M. Tajbakhsh, M. Farhang, Comptes Rendus Chim. **17**, 1160–1164 (2014). https://doi.org/10.1016/j.crci.2013.12.005
26. A. Khalafi-Nezhad, S. Mohammadi, A.C.S. Comb, Science **9**, 512–518 (2013). https://doi.org/10.1021/co400080z
27. A. Deepthi, N.V. Thomas, V. Sathi, Curr. Green Chem. **6**, 210–225 (2019). https://doi.org/10.2174/2213346106666191019144116
28. M. Bashkar, M. Bavadi, E. Ghaderi, K. Niknam, Mol. Divers. **25**, 2001–2015 (2021). https://doi.org/10.1007/s11030-020-10091-5
29. M.M. Li, C.S. Duan, Y.Q. Yu, D.Z. Xu, Dye. Pigment. **150**, 202–206 (2018). https://doi.org/10.1016/j.dyepig.2017.12.007
30. H. Hassani, A. Nozarie, Asian J. Green Chem. **3**, 59–69 (2018). https://doi.org/10.22631/ajgc.2017.101572.1032
31. A. Allahresani, B. Taheri, M.A. Nasseri, Res. Chem. Intermed. **44**, 1173–1188 (2018). https://doi.org/10.1007/s11164-017-3160-8
32. A. Bazgir, G. Hosseini, R. Ghahremanzadeh, A.C.S. Comb, ACS Comb. Sci. **15**, 530–534 (2013). https://doi.org/10.1021/co400057h
33. M. Rouhi, B. Sadeghi, M. Moslemin, Bulg. Chem. Commun. **50**, 23–28 (2018)
34. S.G. Azarnier, M. Esmkhani, Z. Dolatkhah, S. Javanshir, Res. Sq. (2022). https://doi.org/10.1038/s41598-022-10102-5
35. S. Saneinezhad, L. Mohammadi, V. Zadsirjan, F.F. Bamoharram, M.M. Heravi, Sci. Rep. **10**, 1–26 (2020). https://doi.org/10.1038/s41598-020-70738-z
36. B. Karmakar, A. Nayak, J. Banerji, Tetrahedron Lett. **53**, 5004–5007 (2012). https://doi.org/10.1016/j.tetlet.2012.07.030
37. Y.K. Tailor, S. Khandelwal, K. Verma, R. Gopal, M. Kumar, ChemistrySelect **2**, 5933–5941 (2017). https://doi.org/10.1002/slct.201700648
38. A. Rauof, M. Ali, Eng. Technol. Q. Rev. **3**, 45–51 (2020). https://doi.org/10.5281/zenodo.3940869
39. N. Mohammadian, B. Akhlaghinia, Res. Chem. Intermed. **45**, 4737–4756 (2019). https://doi.org/10.1007/s11164-019-03860-x
40. K. Hemmat, M.A. Nasseri, A. Allahresani, S. Ghiami, J. Organomet. Chem. **903**, 120996 (2019). https://doi.org/10.1016/j.jorganchem.2019.120996
41. G. Shanthi, G. Subbulakshmi, P.T. Perumal, Tetrahedron **63**, 2057–2063 (2017). https://doi.org/10.1016/j.tet.2006.12.042
42. M.A. Nasseri, B. Zakerinasab, Res. Chem. Intermed. **41**, 5261–5270 (2015). https://doi.org/10.1007/s11164-014-1627-4
43. H.M. Meshram, D.A. Kumar, B.R.V. Prasad, P.R. Goud, Helv. Chim. Acta **93**, 648–653 (2019). https://doi.org/10.1002/hlca.200900273
44. S.L. Zhu, S.J. Ji, Y. Zhang, Tetrahedron **63**, 9365–9372 (2007). https://doi.org/10.1016/j.tet.2007.06.113
45. M. Dabiri, M. Bahramnejad, M. Baghbanzadeh, Tetrahedron **65**, 9443–9447 (2009). https://doi.org/10.1016/j.tet.2009.08.070
46. A. Mobinikhaledi, N. Foroughifar, M.A.B. Fard, Synth. Commun. **41**, 441–450 (2011). https://doi.org/10.1080/00397911003587507
47. A.R. Khorrami, P. Kiani, A. Bazgir, Monatshefte furr Chem. **142**, 287–295 (2011). https://doi.org/10.1007/s00706-011-0446-1
48. Y. Li, H. Chen, C. Shi, D. Shi, S. Ji, J. Comb. Chem. **12**, 231–237 (2010). https://doi.org/10.1021/cc9001185

49. D.R. Chandam, A.G. Mulik, D.R. Patil, M.B. Deshmukh, Res. Chem. Intermed. **42**, 1411–1423 (2016). https://doi.org/10.1007/s11164-015-2093-3
50. A. Gharib, N.N. Pesyan, B.R.H. Khorasani, M. Roshani, J.W. Scheeren, Bulg. Chem. Commun. **45**, 371–378 (2013)
51. J. Safaei-Ghomi, M. Tavazo, H. Shahbazi-Alavi, Zeitschrift fur Naturforsch.—Sect. B J. Chem. Sci. **74**, 733–738 (2019). https://doi.org/10.1515/znb-2019-0091
52. A. Maleki, N. Ghamari, M. Kamalzare, RSC Adv. **4**, 9416–9423 (2014). https://doi.org/10.1039/C3RA47366J
53. A. Maleki, M. Aghaei, N. Kamalzare, Int. J. Nanosci. Nanotechnol. **12**, 215–222 (2016)
54. J. Safari, S.H. Banitaba, S.D. Khalili, Ultrason. Sonochem. **20**, 401–407 (2013). https://doi.org/10.1016/j.ultsonch.2012.07.007
55. D. Nagargoje, P. Mandhane, S. Shingote, P. Badadhe, C. Gill, Ultrason. Sonochem. **19**(1), 94–96 (2012). https://doi.org/10.1016/j.ultsonch.2011.05.009
56. J. Singh, M. Srivastava, J. Dutta, P.K. Dutta, Int. J. Biol. Macromol. **48**, 170–176 (2011). https://doi.org/10.1016/j.ijbiomac.2010.10.016
57. G. Yin Li, Y. Ren Jiang, K. Long Huang, P. Ding, J. Chen, J. Alloys Compd. **466**, 451–456 (2008). https://doi.org/10.1016/j.jallcom.2007.11.100
58. J.P. Chen, P.C. Yang, Y.H. Ma, T. Wu, Carbohydr. Polym. **84**, 364–372 (2011). https://doi.org/10.1016/j.carbpol.2010.11.052
59. P. Saluja, K. Aggarwal, J.M. Khurana, Synth. Commun. **43**, 3239–3246 (2013). https://doi.org/10.1080/00397911.2012.760130
60. M. Esmaeilpour, A.R. Sardarian, J. Javidi, Appl. Catal. A Gen. **445**, 359–367 (2012). https://doi.org/10.1016/j.apcata.2012.09.010
61. G. Nabiyouni, M. Julaee, D. Ghanbari, P.C. Aliabadi, N. Safaie, J. Ind. Eng. Chem. **21**, 599–603 (2015). https://doi.org/10.1016/j.jiec.2014.03.025